

Hadron Production at RHIC-PHENIX

Tatsuya CHUJO^{*)} for the PHENIX Collaboration

*RIKEN (The Institute of Physical and Chemical Research), Wako, Saitama
351-0198, Japan*

The recent results on hadron production in Au+Au, p+p and d+Au collisions at $\sqrt{s_{NN}} = 200$ GeV from the PHENIX experiment at the BNL-RHIC are summarized. The single particle spectra and yields of identified charged hadrons and neutral pions, two-particle HBT correlations for charged pions, elliptic flow measurements are presented.

§1. Introduction

The physics motivation of the ultra-relativistic heavy-ion program at the Relativistic Heavy Ion Collider (RHIC) is to study nuclear matter at extremely high temperature and energy density with the hope to reach a new form of matter called the quark gluon plasma (QGP). Among the various probes of the QGP state, hadrons carry important information about the collision dynamics along with the spatial and temporal evolution of the system from the early stage of the collisions to the final state interactions. In this report, the recent results on hadron production in Au+Au, p+p and d+Au collisions at $\sqrt{s_{NN}} = 200$ GeV from the PHENIX experiment at the BNL-RHIC are summarized. We will cover the results on single particle spectra and yields of identified charged hadrons and neutral pions, two-particle HBT correlations for charged pions, elliptic flow measurements over a broad p_T range.

§2. PHENIX Experiment

For studies of hadron physics at RHIC, the PHENIX experiment¹⁾ demonstrates good capability for particle identification (PID) for both charged hadrons (π^\pm , K^\pm , p , \bar{p} , d and \bar{d}) and neutral pions over a broad momentum range. The charged hadrons can be identified with time-of-flight measurements in two different detectors: (1) a high resolution Time-of-Flight wall (TOF) and, (2) an electro-magnetic calorimeter (EMC), in conjunction with the tracking system in the PHENIX central arm spectrometers and the beam counter (BBC), which provides the start timing and the event vertex determination. The tracking system in the central arm consists of drift chambers (DC), three layers of pad chambers (PC), and time expansion chambers (TEC). The PHENIX central arms cover $|\eta| < 0.35$ in pseudo-rapidity, and cover $\pi/4$ with the TOF and $3\pi/4$ by EMC in azimuth. The π/K and K/p separation can be achieved up to 2 and 4 GeV/ c in p_T , respectively, using the TOF detector, which has a 115 ps timing resolution. The EMC offers a larger azimuthal coverage for PID, but suffers from a timing resolution of 500 ps. Neutral pions are identified

^{*)} E-mail: chujo@bnl.gov

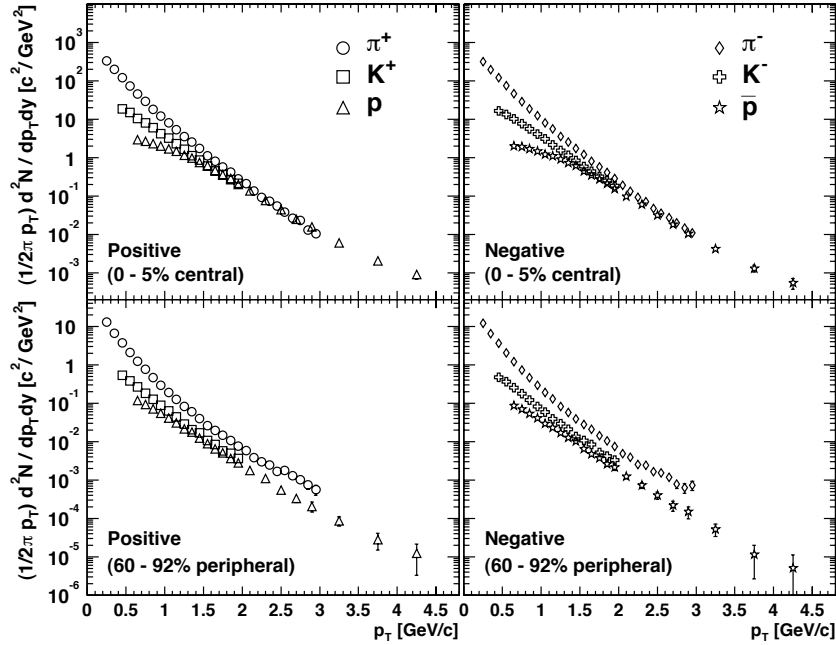


Fig. 1. Transverse momentum distributions for pions, kaons and p , \bar{p} in the 0–5% most central events (upper panels) and 60–91.4% most peripheral events (lower panels) at $\sqrt{s_{NN}} = 200$ GeV in Au+Au collisions³⁾.

with the EMC via the $\pi^0 \rightarrow \gamma\gamma$ decay channel up to 10 GeV/c in p_T using the full statistics taken during the 2nd year of RHIC run in Au+Au collisions.

We use the PHENIX minimum bias trigger events, which include $92.2^{+2.5}_{-3.0}\%$ of the 6.9 barn Au+Au total inelastic cross section²⁾. For the collision centrality determination, these events are subdivided using the BBC and ZDC correlation. Based on a Glauber model calculation²⁾ two global quantities to characterize the event centrality are used: the average number of participants $\langle N_{part} \rangle$ and the average number of collisions $\langle N_{coll} \rangle$ associated with each centrality bin. The data presented here were taken during RHIC runs with Au+Au and p+p at $\sqrt{s_{NN}} = 200$ GeV in 2001-2002 and d+Au at $\sqrt{s_{NN}} = 200$ GeV in 2002-2003.

§3. Identified Single Particle Spectra

The transverse momentum distributions of identified particle can be used to characterize the bulk properties of created matter at the freeze-out state when the produced hadrons no longer strongly interact with each other. Fig. 1 shows the p_T distributions for pions, kaons, protons, and anti-protons at mid-rapidity in Au+Au collisions at $\sqrt{s_{NN}} = 200$ GeV³⁾. The top two plots are for the most central 0–5% collisions, and the bottom two are for the most peripheral 60–92% collisions. The

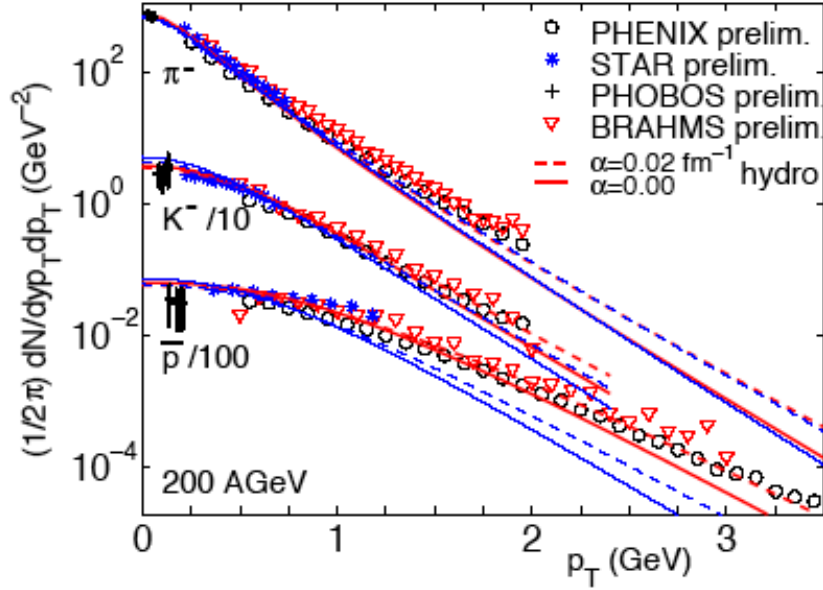


Fig. 2. Transverse momentum spectra for π^- , K^- and \bar{p} for central Au+Au collisions at $\sqrt{s_{NN}} = 200$ GeV from all RHIC experiments compared with a hydrodynamical model calculation⁵⁾.

spectra for positive particles are presented on the left, and those for negative particles on the right. For $p_T < 1.5$ GeV/ c in central events, the data show a clear mass dependence in the shapes of the spectra. The p and \bar{p} spectra have a shoulder-arm shape, the pion spectra have a concave shape, and the kaons fall exponentially. On the other hand, in the peripheral events, the mass dependences of the p_T spectra are less pronounced and the p_T spectra are more nearly parallel to each other. Another notable observation is that at p_T above ≈ 2.0 GeV/ c in central events, the p and \bar{p} yields become comparable to the pion yields, which is also observed in 130 GeV Au+Au collisions⁴⁾. This observation shows that a significant fraction of the total particle yield at $p_T \approx 2.0 - 4.5$ GeV/ c in Au+Au central collisions consists of p and \bar{p} . The observed mass dependence of spectra shape is consistent with a collective hydrodynamical expansion picture. As shown in Fig. 2, a Hydrodynamic model⁵⁾ agrees well with the data from all four RHIC experiments in central collisions up to 1.5 – 2 GeV for pions and up to a least 3 GeV for protons.

Within the framework of the statistical thermal model⁶⁾ in a grand canonical ensemble with baryon number, strangeness and charge conservation⁷⁾, particle ratios measured at $\sqrt{s_{NN}} = 130$ GeV at mid-rapidity have been analyzed with the extracted chemical freeze-out temperature $T_{ch} = 174 \pm 7$ MeV and baryon chemical potential $\mu_B = 46 \pm 5$ MeV. A set of chemical parameters at $\sqrt{s_{NN}} = 200$ GeV in Au+Au were also predicted by using a phenomenological parameterization of the energy dependence of μ_B . The predictions were $\mu_B = 29 \pm 8$ MeV and $T_{ch} = 177 \pm 7$ MeV at $\sqrt{s_{NN}} = 200$ GeV. The comparison between data at 130 (200) GeV for central

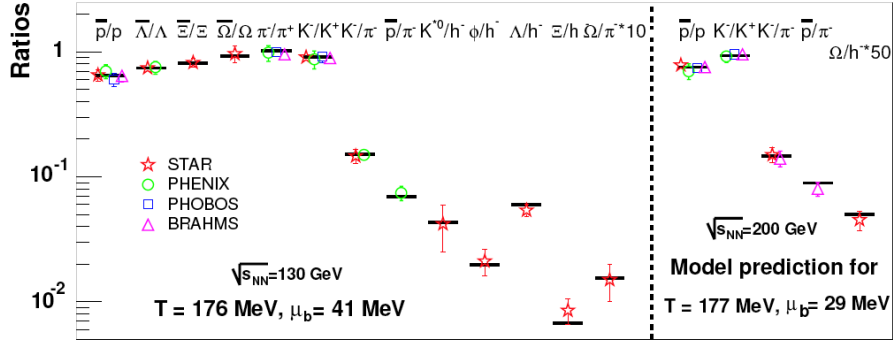


Fig. 3. Comparison of PHENIX particle ratios with those of PHOBOS, BRAHMS and STAR results in Au+Au central collisions at $\sqrt{s_{NN}} = 130$ and 200 GeV at mid-rapidity. The thermal model prediction⁷⁾ central collisions are also shown as solid lines.

collisions and the thermal model prediction is shown in Fig. 3. There is a good agreement between data and the model. The small μ_B is qualitatively consistent with our measurement of the number of net protons (≈ 5) in central Au+Au collisions at $\sqrt{s_{NN}} = 200$ GeV at mid-rapidity³⁾.

§4. Two-Particle HBT Correlation

Another way to extract information about the particle emitting source created in relativistic heavy ion collisions is with two-particle intensity interferometry or the Hanbury-Brown Twiss (HBT) correlations. The HBT measurement is sensitive to the space-time evolution and duration time of the system at the freeze-out stage. In this analysis the Bertsch-Pratt parameterization is employed in a Longitudinal Center-of-Mass System (LCMS), where the three-dimensional Gaussian radius parameters are R_{side} , R_{out} and R_{long} . These radius parameters are studied as a function of the transverse momentum of the pairs (k_T) and centrality. The charged pions are identified by the time-of-flight measurement in the EMC. A full Coulomb correction is applied assuming a Gaussian source and no pairs coming from resonance decays.

As shown in reference⁸⁾, we have observed a clear k_T dependence for all Bertsch-Pratt radius parameters for pions in 200 GeV Au+Au collisions. This k_T dependence of the radius parameters can be explained by a space-momentum correlation effect due to the expansion of the system⁹⁾. For the study of the duration time of the system, the ratio R_{out}/R_{side} can be used. In Fig. 4, the ratio R_{out}/R_{side} as a function of k_T and N_{part} for charged pion pairs is shown. The ratio does not change as a function of both k_T and centrality within the experimental uncertainties. In contrast to the success of the hydrodynamic model for p_T distributions of identified charged particle and elliptic flow at low p_T , the HBT radii from the hydrodynamic calculation agree only qualitatively with the data with significant quantitative discrepancies¹⁰⁾. This discrepancies between data and the hydrodynamic models is known as so-called “RHIC HBT puzzle”. It is also pointed out that the discrepancy may be resolved by

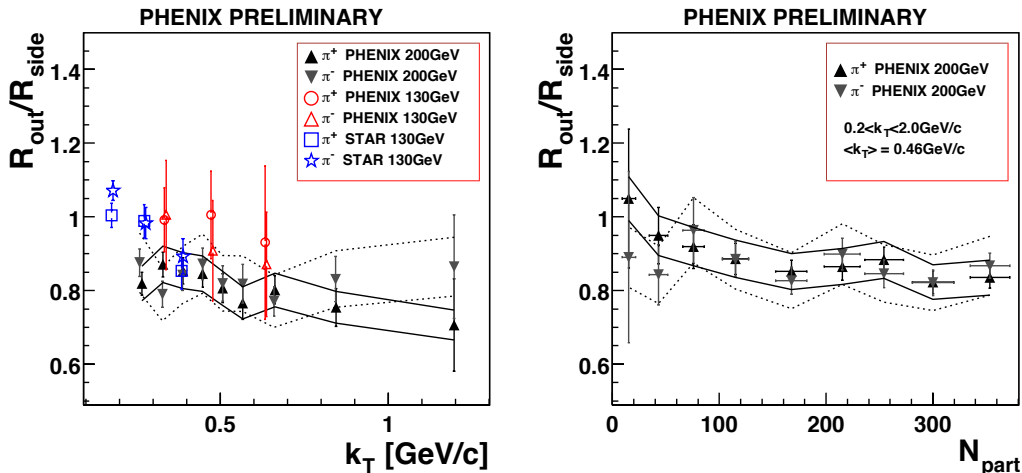


Fig. 4. The ratio R_{out}/R_{side} as a function of k_T (left) and N_{part} (right)⁸⁾. STAR data points from the reference¹²⁾.

the introducing a Core-Halo picture¹¹⁾ of the source and assumes that the fraction of pairs are the only pairs that contribute to the Coulomb interaction^{*)}.

§5. Elliptic Flow

In non-central collisions, the initial overlap region of two nuclei is elliptically deformed in the transverse plane, resulting in anisotropic pressure gradients. These cause a more rapid expansion into the reaction plane than perpendicular to it, resulting in an anisotropy of the final p_T distributions called elliptic flow¹⁰⁾. Since the event anisotropy is considered to be developed at the early stage of collisions, the study of elliptic flow provides a good tool to investigate the possible formation of a QGP state.

Elliptic flow is quantified by the second harmonic coefficient (v_2) of a Fourier expansion in the azimuthal distributions of the measured spectrum with respect to the reaction plane. We have measured the v_2 parameter for identified particles with respect to the reaction plane, which is defined in the beam counters ($|\eta| = 3 \sim 4$) in 200 GeV Au+Au collisions. The details of the analysis method and results are found in¹³⁾. At low p_T ($< 2 \text{ GeV}/c$) the strength of the elliptic flow signal is found to be large and consistent with hydrodynamics calculations. Above $p_T \approx 2 \text{ GeV}/c$, the data deviate from the hydrodynamic calculations for both mesons and baryons. In addition, the model cannot reproduce the opposite mass dependence of the v_2 parameter, which is observed above $2 \text{ GeV}/c$. Various interpretations have been proposed to account for such a large v_2 parameter and their complicated

*) Most recent results using the partial Coulomb corrections are found in S.S.Adler, nucl-ex/0401003.

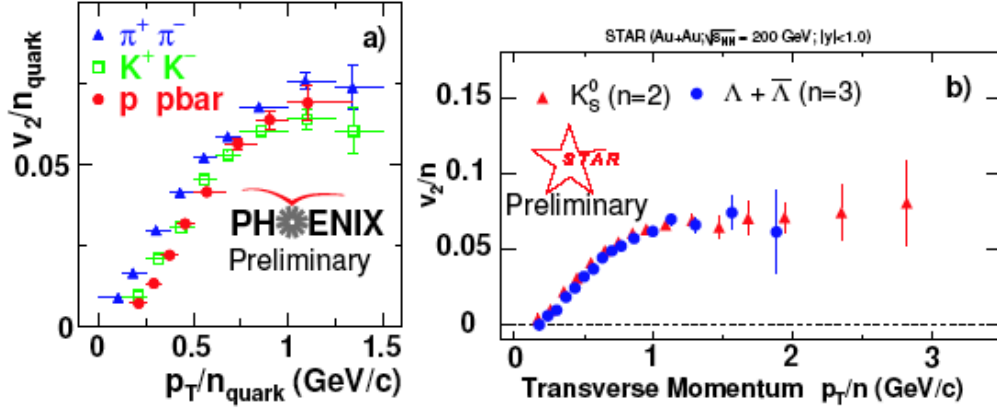


Fig. 5. Transverse momentum dependence of v_2 for charged pions, charged kaons and protons plus anti-protons by PHENIX¹³⁾, and Λ and K_s^0 by STAR¹⁵⁾. Shown is v_2 versus p_T where both are normalized by the number of constituent quarks. The figure is taken from the reference¹⁶⁾.

flow pattern for different particle type. Quark coalescence models¹⁴⁾ naturally lead to this flow pattern. Fig. 5 shows the p_T/n dependence of the v_2/n , where n is the number of constituent quarks ($n=2$ for mesons, $n=3$ for baryons), for charged pions, charged kaons and protons plus anti-protons by PHENIX¹³⁾, and Λ plus $\bar{\Lambda}$ and K_s^0 by STAR¹⁵⁾. It is found that they globally fall in a single curve, supports the scenario where hadrons at moderate p_T form by the coalescence of co-moving quarks.

§6. High p_T Hadron Yield Suppression

While the bulk of the particles produced in the relativistic heavy-ion collisions are produced in the late hadronization phase of the collisions, high transverse momentum ($p_T > 2$ GeV/c) hadrons arise from the fragmentation of partons (quarks and gluons) produced in parton-parton scattering with large momentum transfer (hard processes) during the initial phase of the collisions. While the scattered partons in proton-proton interactions propagate through the normal QCD vacuum before the fragmentation into hadrons, in nucleus-nucleus collisions, the partons from hard scattering must propagate through the surrounding dense medium. As they traverse the dense matter, the partons will interact with it losing energy before fragmenting into the observed hadrons in the final state (jet quenching). Thus, the magnitude of the jet quenching effect in terms of parton energy loss, or corresponding suppression of the high p_T particle yields thus provide a means to probe the created matter¹⁷⁾.

The nuclear medium effects on high p_T production can be quantified by the nuclear modification factor, R_{AB} , defined for collisions of A+B as the ratio of invariant yield in A+B to that of p+p, scaled by the number of binary collisions.

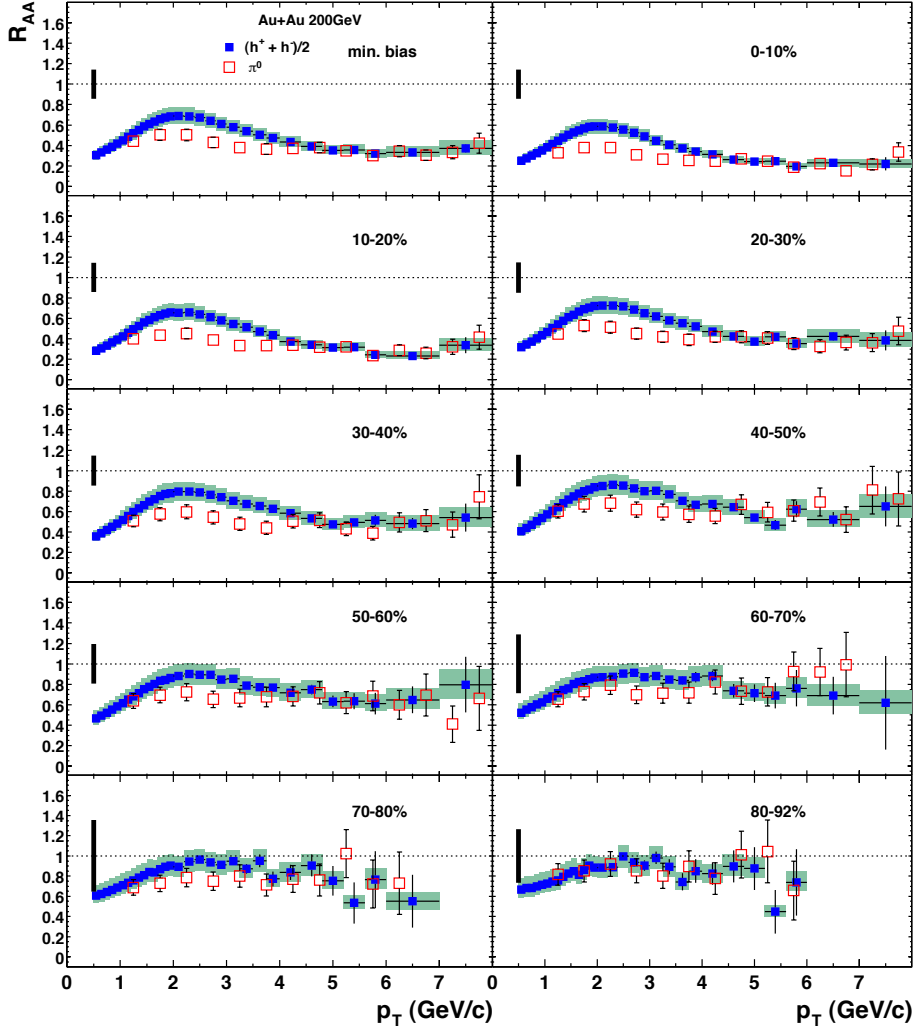


Fig. 6. The nuclear modification factors $R_{AA}(p_T)$ for π^0 and charged hadrons in different centrality bins in Au+Au collisions at $\sqrt{s_{NN}} = 200$ GeV^{2), 18)}.

$$R_{AB}(p_T) = \frac{(1/N_{AB}^{evt})d^2N_{AB}/d\eta dp_T}{\langle N_{coll} \rangle / \sigma_{pp}^{inel} d^2\sigma_{pp}/d\eta dp_T} = \frac{(1/N_{AB}^{evt})d^2N_{AB}/d\eta dp_T}{\langle T_{AB} \rangle d^2\sigma_{pp}/d\eta dp_T}, \quad (6.1)$$

where $\langle N_{coll} \rangle$ is the average number of inelastic nucleon-nucleon collisions per event, and $\langle T_{AB} \rangle = \langle N_{coll} \rangle / \sigma_{pp}^{inel}$ is the average of the nuclear overlap function, which is determined purely from the nuclear geometry. Thus $\langle T_{AB} \rangle$ represents the parton luminosity and $\langle T_{AB} \rangle d^2\sigma_{pp}/d\eta dp_T$ gives the expected yield for the experimentally selected nuclear geometry. For heavy-ion collisions, R_{AB} is expected to be below unity at low p_T where the bulk of the particle production is due to soft processes which scale like the overlap volume, or number of participant nucleons $\langle N_{part} \rangle$, rather than as $\langle N_{coll} \rangle$. At high p_T however, R_{AB} should be unity in the absence of nuclear

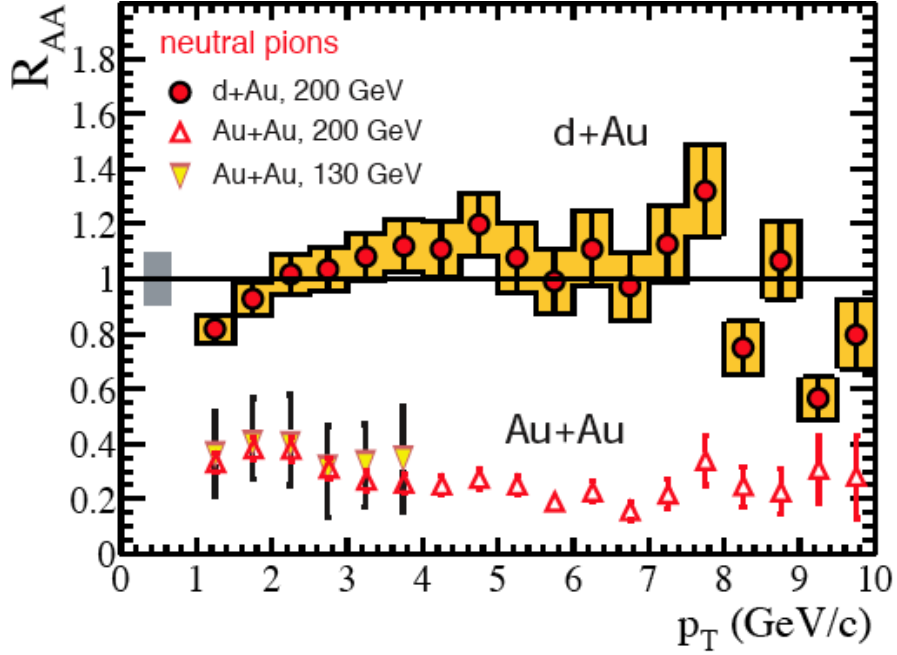


Fig. 7. Comparison of the p_T dependence of the nuclear modification factor R_{AB} for π^0 's in minimum bias d+Au collisions and central Au+Au collisions at $\sqrt{s_{NN}} = 130$ and 200 GeV²¹⁾.

medium effects.

In Fig. 6, the nuclear modification factors R_{AA} for π^0 and charged hadrons in different centrality bins in Au+Au collisions at $\sqrt{s_{NN}} = 200$ GeV are shown^{2), 18), 19)}. For peripheral collisions, it scales as the number of binary collisions for all measured p_T range. For the central collisions, we found the factor of ≈ 5 suppression and it extends up to $p_T = 8$ GeV/c. On the other hand, initial state effects such as nuclear modifications to the parton momentum distributions, and soft processes expected by the incoming parton prior to its hard scattering, could also contribute. In fact, interpretations of the Au+Au results based on initial state gluon saturation effects²⁰⁾ also predict a considerable suppression of the hadron production at high p_T .

§7. The d+Au Control Experiment

In order to distinguish between an initial state effect such as gluon saturation and a final state effect for the observed suppression, d+Au collisions at $\sqrt{s_{NN}} = 200$ GeV were studied at RHIC²¹⁾. While initial state nuclear effects will be present in the d+Au system, there will be no large hot dense medium produced. Thus if the hadron suppression is due to parton energy loss in the produced matter (final state effect), the suppression should not be observed in d+Au system. In Fig. 7, the nuclear modification factor R_{dA} is shown for neutral pions compared to the results for central Au+Au collisions. It is seen that there is no suppression of high p_T particles in d+Au collisions, but rather the yield is slightly enhanced for $p_T > 2$

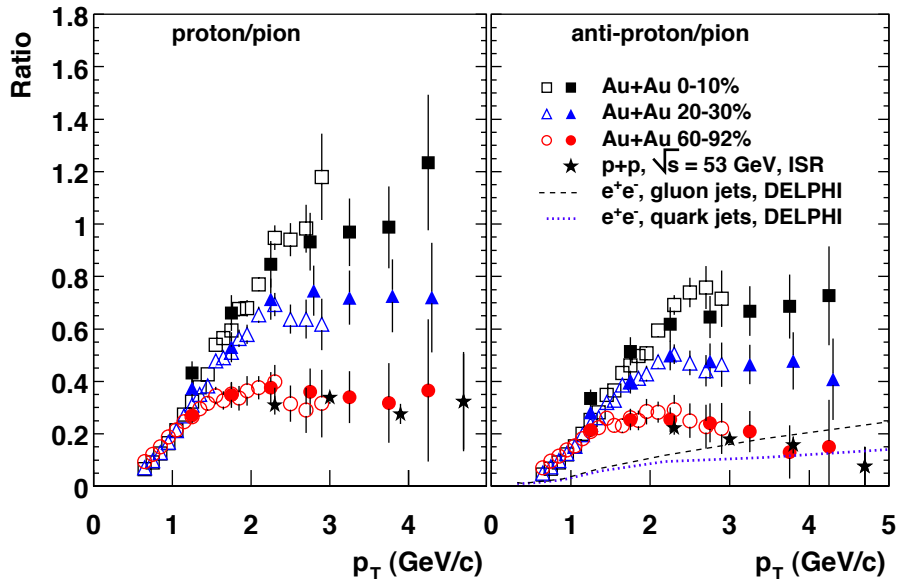


Fig. 8. Centrality dependence of p/π and \bar{p}/π ratios in Au+Au collisions at $\sqrt{s_{NN}} = 200$ GeV^{3), 23)}.

GeV/ c , similar to observations at lower incident energies for p+A collisions²²⁾. The results strongly indicate that the suppression in central Au+Au collisions is not an initial state effect, but instead is most likely a final state effect due to the produced dense medium.

§8. Proton at Intermediate p_T

Fig. 8 shows the p/π and \bar{p}/π ratios as a function of p_T measured at mid-rapidity in different collision centrality selections in Au+Au at $\sqrt{s_{NN}} = 200$ GeV. We observed that there is a strong centrality dependence in p/π and \bar{p}/π ratios at the intermediate p_T region, *i.e.*, the ratios in central events are a factor of ~ 3 larger than in peripheral events. The peripheral data at $p_T > 3$ GeV/ c agrees well with the ratios observed in p+p collisions at lower energies and the results from gluon and quark jet fragmentation. In order to investigate the scaling behavior and yield suppression effect for p and \bar{p} , the N_{coll} scaled central to peripheral yield ratios (R_{CP}) for protons is used. As shown in Fig. 9, p and \bar{p} are not suppressed at $p_T = 1.5 - 4.5$ GeV/ c while there is a factor of 2 – 3 suppression for π^0 . We also observe that h/π^0 ratio in central events is enhanced by as much as 50% above the p+p value²³⁾ and this relative baryon enhancement is limited to $p_T < 5-6$ GeV/ c .

It is interesting why the suppression for p and \bar{p} is absent in central Au+Au collisions. Recently the observed abundance of protons yields relative to pions in central collisions has been attributed to the recombination of quarks, rather than fragmentation²⁴⁾. In this model, quark recombination for p and \bar{p} is effective up to $p_T \simeq 5$ GeV above which fragmentation dominates for all particle species. Another explanation of the observed large baryon content invokes a hydrodynamical radial flow and the jet quenching of hard jet²⁵⁾. Both theoretical models agree with data

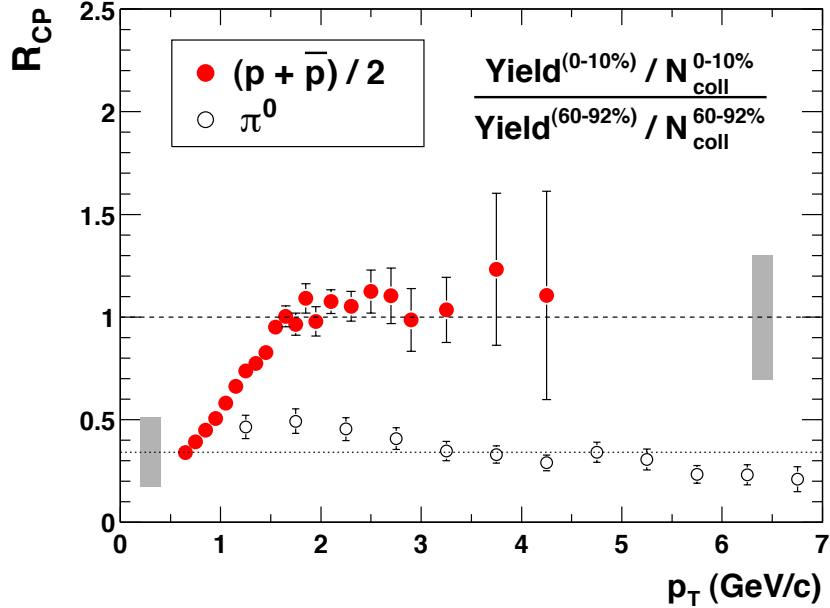


Fig. 9. Nuclear modification factor R_{CP} for $(p+\bar{p})/2$ and π^0 ^{3), 23)}. Dashed and dotted lines indicate N_{coll} and N_{part} scaling; the shaded bars show the systematic errors on these quantities.

qualitatively and predict that the baryon/meson enhancement is limited to $p_T < \sim 5$ GeV/ c .

§9. Summary

We present results on hadron production in p+p, d+Au and Au+Au collisions at $\sqrt{s_{NN}} = 200$ GeV at mid-rapidity over a broad momentum range from the PHENIX experiment. The transverse momentum distributions for π^\pm , K^\pm , p and \bar{p} are measured and we observe a mass dependence of the slopes and shapes of the identified charged spectra in central events. In two-particle HBT correlations for charged pions, there is a clear k_T dependence of all radius parameters. These results on the single particle spectra and two-particle HBT correlations are qualitatively consistent with a hydrodynamic collective expanding source picture, although there are quantitative discrepancies between the model and the HBT results. It is also found that the all particle ratios at central Au+Au collisions at RHIC energies agree with the thermal model expectations.

The data on elliptic flow with respect to the reaction plane shows that at low p_T (< 2 GeV/ c) the light mesons have a larger v_2 parameter compared to protons and \bar{p} . The hydrodynamic model calculation agrees very well with the data for all particles up to 2 GeV/ c . However, the data seems to deviate from the hydrodynamic model above 2 GeV/ c for both mesons and baryons. The model cannot reproduce the opposite mass dependence of the v_2 parameter above 2 GeV/ c . This complicated flow pattern seems to be naturally explained by a parton coalescence picture.

At high p_T central Au+Au collisions, there is a factor of 4 – 5 suppression for neutral pion and charged hadron yield, compared to expectations from scaled p+p results. No suppression of high p_T particles is observed in d+Au collisions, suggesting that the observed suppression in central Au+Au collisions is due to the produced dense matter. For the proton and anti-proton production, we found the relative baryon enhancement at intermediate p_T compared to that of pion. The yields p and \bar{p} are not suppressed at $p_T = 1.5 - 4.5$ GeV/ c while there is a factor of 2 – 3 suppression for π^0 . This observation has been attributed to the recombination model and invokes a hydrodynamical radial flow plus jet model. Both theoretical models agree with data qualitatively and predict that the baryon/meson enhancement is limited to $p_T < \sim 5$ GeV/ c .

References

- 1) PHENIX Collaboration, K. Adcox *et al.*, Nucl. Instrum. Methods A **499**, 469 (2003) and the references therein.
- 2) S.S. Adler *et al.*, Phys. Rev. Lett. **91**, 072301 (2003).
- 3) S.S. Adler *et al.*, Submitted to Phys. Rev. C, nucl-ex/0307022.
- 4) K. Adcox *et al.*, Phys. Rev. Lett. **88**, 242301 (2002).
- 5) P.F. Kolb and R. Rapp, Phys. Rev. C **67**, 044903 (2003).
- 6) F. Becattini *et al.*, hep-ph/0002267.
- 7) P.Braun-Munzinger, D.Magestro, K.Redlich, J.Stachel, Phys. Lett. B **518**, 41 (2001).
- 8) A. Enokizono, PHENIX Collaboration, Nucl. Phys. A **715**, 595c (2003).
- 9) Y. F. Wu *et al.*, Eur. Phys. J. C **1**, 599 (1998).
- 10) U. Heinz and P.F. Kolb, hep-ph/0204061.
- 11) Y. M. Sinyukov *et al.*, Phys. Lett. B **432**, 248 (1998); T. Csörgö *et al.*, Eur. Phys. J. C **9**, 275 (1999).
- 12) C. Adler *et al.*, Phys. Rev. Lett. **87**, 082301 (2001).
- 13) S.S. Adler *et al.*, Phys. Rev. Lett. **91**, 182301 (2003).
- 14) D. Molnar and S. A. Voloshin, Phys. Rev. Lett. **91**, 092301 (2003).
- 15) J. Adams *et al.*, nucl-ex/0306007.
- 16) R. Snellings, nucl-ex/0310019.
- 17) M. Gyulassy and M. Plümer, Phys. Lett. B **243**, 432 (1990); X. N. Wang and M. Gyulassy, Phys. Rev. Lett. **68**, 1480 (1992).
- 18) S.S. Adler *et al.*, Submitted to Phys. Rev. C, nucl-ex/0308006.
- 19) S.S. Adler *et al.*, Phys. Rev. Lett. **91**, 241803 (2003).
- 20) D. Kharzeev, E. Levin and L. McLerran, Phys. Lett. B **561**, 93 (2003).
- 21) S.S. Adler *et al.*, Phys. Rev. Lett. **91**, 072303 (2003).
- 22) D. Antreasyan *et al.*, Phys. Rev. D **19**, 764 (1979).
- 23) S.S. Adler *et al.*, Phys. Rev. Lett. **91**, 172301 (2003).
- 24) R. C. Hwa *et al.*, Phys. Rev. C **67**, 034902 (2003); R. J. Fries *et al.*, nucl-th/0301087; V. Greco *et al.*, nucl-th/0301093.
- 25) T. Hirano and Y. Nara, nucl-th/0307015.